

Manipulating non-Hermitian skin effect via electric fields

Yi Peng,^{1,2,3,*} Jianwen Jie,^{1,2,3,*} Dapeng Yu,^{1,2,3} and Yucheng Wang^{1,2,3,†}

¹Shenzhen Institute for Quantum Science and Engineering,
Southern University of Science and Technology, Shenzhen 518055, China

²International Quantum Academy, Shenzhen 518048, China

³Guangdong Provincial Key Laboratory of Quantum Science and Engineering,
Southern University of Science and Technology, Shenzhen 518055, China

In non-Hermitian systems, the phenomenon that the bulk-band eigenstates are accumulated at the boundaries of the systems under open boundary conditions is called non-Hermitian skin effect (NHSE), which is one of the most iconic and important features of a non-Hermitian system. In this work, we investigate the fate of NHSE in the presence of electric fields by analytically calculating the dynamical evolution of an initial bulk state and numerically computing the spectral winding number, the distributions of eigenstates, as well as the dynamical evolutions. We show abundant manipulation effects of dc and ac fields on the NHSE, and that the physical mechanism behind these effects is the interplay between the Stark localization, dynamic localization and the NHSE. In addition, the finite size analysis of the non-Hermitian system with a pure dc field shows the phenomenon of size-dependent NHSE. We further propose a scheme to realize the discussed model based on an electronic circuit. The results will help to deepen the understanding of NHSE and its manipulation.

Introduction.— Hermiticity of Hamiltonian has been regarded as a fundamental requirement in standard quantum mechanics, and it ensures the conservation of probability and limits energy-values to be real in isolated systems. However, many systems, such as the nonequilibrium and open systems with gain and loss, can be effectively described by non-Hermitian Hamiltonians. Especially in recent years, non-Hermitian physics has attracted widespread attention in both theory [1–16] and experiment [17–24]. Various unique features of non-Hermitian systems without any Hermitian counterparts have been revealed, such as exceptional points and rings [25–34], enriched topological classifications [35–40], and non-Hermitian skin effect (NHSE) [7, 8, 10, 21, 41–46]. NHSE, namely that a majority of eigenstates are localized near the boundary under open boundary conditions (OBC), is one of the most iconic properties of non-Hermitian systems. It drastically reshapes the bulk-boundary correspondence principle and motivates the establishment of generalized Brillouin zone [7–9]. The interplay between the NHSE and other fundamental phenomena (e.g., localization induced by external magnetic fields, defects, disorder and quasiperiodic potentials [12–15, 46–50]) has also attracted widespread attentions recently. On the other hand, electric field can induce the Stark localization or dynamical localization, and is also a frequently used fundamental method to manipulate other physical effects, since it is easily realized and controlled. However, the effect of electric fields on NHSE was not considered before.

Now we focus on how to manipulate NHSE by using electric fields. If the NHSE can be fully suppressed in the modulation process, the non-Hermitian effect may be eliminated, and the system may have the conservation of probability and all the eigenvalues may become real, even

though the non-Hermitian term remains. Thus, manipulating NHSE is helpful for deepening our understandings of non-Hermitian quantum mechanics and the differences between Hermitian and non-Hermitian physics. Moreover, mastering how to control NHSE, we will be able to obtain or remove it on demand. Therefore, manipulating NHSE also has practical significance. In this work, we want to address whether electric fields can manipulate NHSE, and furthermore, if they can, whether richer and more interesting physics and applications will emerge in light of this.

Model and results.— We consider a one dimensional non-Hermitian system with non-reciprocal hopping under the influence of electric fields, and the Hamiltonian is written as

$$\hat{H} = \sum_n (J_L|n\rangle\langle n+1| + J_R|n+1\rangle\langle n|) + E(t)a \sum_n n|n\rangle\langle n|, \quad (1)$$

where $|n\rangle$ is the Wannier state localized on the lattice site n , $J_L(J_R)$ represents the leftward (rightward) hopping amplitude, a is the lattice constant, being set as 1 throughout this work, and $E(t) = e\xi(t)$, with e and $\xi(t)$ being the particle's charge and external electric field, respectively.

We can analytically confirm the existence or disappearance of NHSE by investigating the motion of a particle, this is because the particle initially localized in the bulk should move toward the boundary if the NHSE exists. We firstly substitute an arbitrary time-dependent quantum state $|\psi(t)\rangle = \sum_m C_m(t)|m\rangle$ into the Schrödinger equation $i\partial_t|\psi(t)\rangle = \hat{H}(t)|\psi(t)\rangle$ and obtain the equation of motion for the time-dependent amplitudes $C_m(t)$,

$$i\partial_t C_m(t) = J_L C_{m+1}(t) + J_R C_{m-1}(t) + mE(t)C_m(t). \quad (2)$$

Here we set $\hbar = 1$. By solving the Eq. (2), for arbitrary

$E(t)$, we can obtain the exact solutions,

$$C_m(t) = \sum_n (-1)^{m-n} C_n(0) e^{-i\eta(t)n} \mathcal{J}_{m-n} \left(2\sqrt{J_L J_R} [\mathcal{U}^2(t) + \mathcal{V}^2(t)] \right) \left[\frac{J_R i\mathcal{V}(t) - \mathcal{U}(t)}{J_L i\mathcal{V}(t) + \mathcal{U}(t)} \right]^{\frac{m-n}{2}}. \quad (3)$$

Here $\mathcal{J}_{m-n}(x)$ is the $(m-n)$ th order Bessel function of the first kind, $\mathcal{U}(t) = \int_0^t \cos[\eta(t) - \eta(t')] dt'$ and $\mathcal{V}(t) = \int_0^t \sin[\eta(t) - \eta(t')] dt'$ with

$$\eta(t) = \int_0^t E(t') dt'. \quad (4)$$

This solution is valid for arbitrary initial bulk state $|\psi(0)\rangle$ and arbitrary $E(t)$, and the calculation details are in the Supplementary Materials [51]. To simplify the expression, without loss of generality, we consider a specific initial state that only occupy a single Wannier lattice site n_0 , namely $|\psi(0)\rangle = |n_0\rangle$, and then the probability at any site m after evolution time t , $\rho_m(t) = |C_m(t)|^2$, takes [51],

$$\rho_m(t) = \mathcal{J}_{m-n_0}^2 \left(2\sqrt{J_L J_R} [u^2(t) + v^2(t)] \right) \left(\frac{J_R}{J_L} \right)^{m-n_0}, \quad (5)$$

with

$$u(t) = \int_0^t dt' \cos \eta(t'), \quad v(t) = \int_0^t dt' \sin \eta(t'). \quad (6)$$

In the absence of electric fields, i.e., $E(t) = 0$, from Eq. (4) and Eq. (6), we have $u(t) = t$ and $v(t) = 0$, yielding $\rho_m(t) = \mathcal{J}_{m-n_0}^2(2t\sqrt{J_L J_R}) (J_R/J_L)^{m-n_0}$, where $2t\sqrt{J_L J_R}$ linearly increases to infinity and thus $\mathcal{J}_{m-n_0}(2t\sqrt{J_L J_R})$ tends to 0 [52] [see Fig. 1(a)], such that $\rho_m/\rho_{m-1} \approx J_R/J_L$ when $t \rightarrow \infty$ [51]. Therefore, the system has right (left) boundary skin mode when $J_R/J_L > 1$ ($J_R/J_L < 1$), which is consistent with previous results [7, 8, 10]. The following sections will discuss three cases: i) the pure dc field case, ii) the pure ac field case, and iii) the dc-ac mixed field case.

The pure dc electric field case. — We firstly discuss the fate of NHSE in the presence of a pure dc electric field, i.e., $E(t) = E_0$. From Eq. (4) and Eq. (6), we have $u(t) = \sin(E_0 t)/E_0$ and $v(t) = (1 - \cos E_0 t)/E_0$, and then, Eq. (5) gives the probability:

$$\rho_m(t) = \mathcal{J}_{m-n_0}^2 \left(\frac{4\sqrt{J_L J_R}}{E_0} \sin \frac{E_0 t}{2} \right) \left(\frac{J_R}{J_L} \right)^{m-n_0}. \quad (7)$$

Note that $\sin(E_0 t^*/2) = 0$ at the time points $t^* = 2\pi N/E_0$ with $N = 0, 1, 2, \dots$. By using the properties of the Bessel function [52] $\mathcal{J}_{m-n_0}(0) = \delta_{m-n_0,0}$ [see

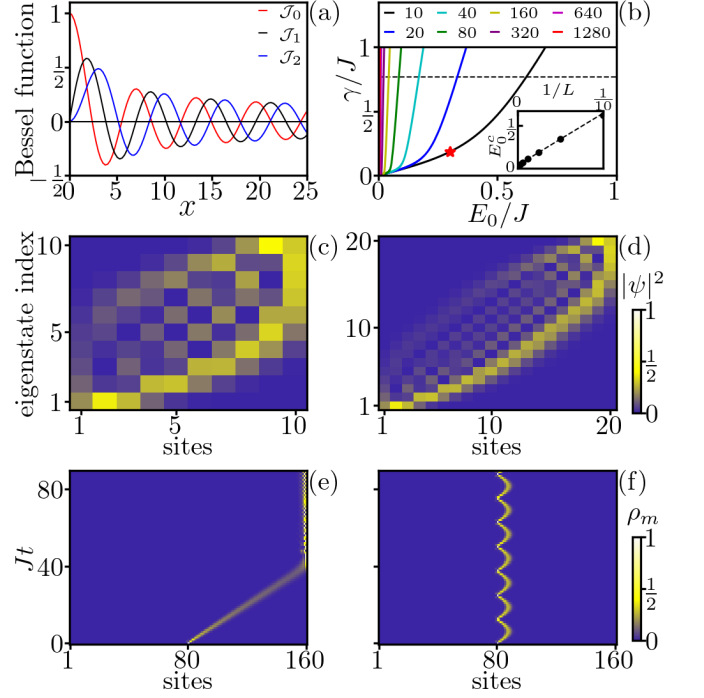


Figure 1: (a) Distributions of the zeroth, first and second order Bessel function. We can see two characteristics used in the text: the amplitudes decrease with increasing x and when $x \rightarrow \infty$, $\mathcal{J}_m(x) \rightarrow 0$ for any m ; $\mathcal{J}_0(0) = 1$ and $\mathcal{J}_m(0) = 0$ when $m \neq 0$, so we have $\mathcal{J}_m(0) = \delta_{m,0}$. (b) Localization-delocalization transition characterized by winding number for finite lattices. The inset shows transition dc field strength E_0^c versus $1/L$, given $\gamma = 0.77$ marked as dashed line in its parent figure. The distributions of eigenstates with (c) $L = 10$ and (d) $L = 20$, and other parameters are $\gamma = 0.185$ and $E_0 = 0.3$ as marked by red star in (b). Dynamical evolution of an electron started from the lattice center under (e) the weak dc field with $E_0 = 0.005$ and (f) the strong dc field with $E_0 = 0.5$, and other parameters are $L = 160$, $\gamma = 0.769$.

Fig. 1(a)] and $(J_R/J_L)^{m-n_0} = 1$ when $m = n_0$, we have that $\rho_{m=n_0}(t^*)$ will oscillate back to 1 whatever the initial site n_0 is, and this phenomenon is called Stark localization [53], which induces that the particle initially localized at the bulk does not move toward the boundary. Therefore, the effect of the interplay between the Stark localization and NHSE is that even a small dc field is sufficient to suppress the NHSE.

The analytical results can be further confirmed by numerically calculating the winding number (WN). To define the WN, we need to introduce the twist boundary condition here, i.e., $\hat{H}(\Phi) = \hat{H} + J_L e^{i\Phi} |L\rangle\langle 1| + J_R e^{-i\Phi} |1\rangle\langle L|$, where L is the system size and Φ is the introduced phase factor, and then the WN reads

$$w = \frac{1}{2\pi i} \int_0^{2\pi} \partial_\Phi \ln \det [\hat{H}(\Phi) - \mathcal{E}_c] d\Phi. \quad (8)$$

$w = 1$ ($w = 0$) corresponds to the existence (non-existence) of NHSE under OBC with eigenvalue around \mathcal{E}_c [6, 42, 43, 45], which is set to the algebra average of the spectrum in the following calculation. For convenience, we set $J_L = J - \gamma/2$ and $J_R = J + \gamma/2$ with $\gamma > 0$ and $J = 1$ as the unit of energy. Fig. 1 (b) shows the transition of the existence-nonexistence of NHSE, obtained by calculating the WN, which changes from 1 to 0 when the strength of dc field E_0 increases cross the transition line with fixed L from left to right. It can be seen that the transition lines tend to $E_0 = 0$ with increasing L , which is consistent with the analytical result.

The analytical expression of $\rho_m(t)$ can also tell us the finite size effect, where interesting physics will emerge. Here, we consider $J_R > J_L$, which makes the oscillation of the particle favor the right-hand side of the initial position n_0 , and the oscillation range is approximate to $4J_R/|E_0|x_\star$ [51], where x_\star only depends on J_L and J_R . If the distance between the right-side boundary and n_0 is larger than $4J_R/|E_0|x_\star$, the particle will return back to n_0 after a period of time, but if the distance is less than $4J_R/|E_0|x_\star$, the particle will arrive at the boundary and then stay there ever since. Thus, for fixed size L , there exist a critical electric field strength E_0^c that describes the transition of the existence-nonexistence of NHSE and satisfies $4J_R/|E_0^c|x_\star = L$, giving $E_0^c \propto 1/L$, as shown in the inset of Fig. 1 (b). When the size exceed a critical value, the number of skin modes is about $4J_R/|E_0|x_\star$, being independent of the size. It can be clearly seen by comparing Fig. 1 (c) and (d), which show the distributions of eigenstates with different sizes and same other parameters, and have the same number of skin modes. Thus, with fixing J_L , J_R and E_0 , the number of skin modes can be of the same order of magnitude as the total eigenstate number for the system with small size and the NHSE exists. When the size is large enough, the ratio of the number of skin modes to the total eigenstate number will be insignificant and the NHSE will disappear, suggesting that the NHSE is size-dependent, which is different from the general NHSE. Moreover, we can increase the number of skin modes by decreasing the electric field strength, and thus, we can control the appearance or disappearance of NHSE for a finite size system, as shown in Fig. 1 (e) and (f), where the system shows NHSE when $E_0 = 0.005$, but when $E_0 = 0.5$, the NHSE disappear. The phenomenon of the size-dependent NHSE should widely exist in the non-Hermitian systems

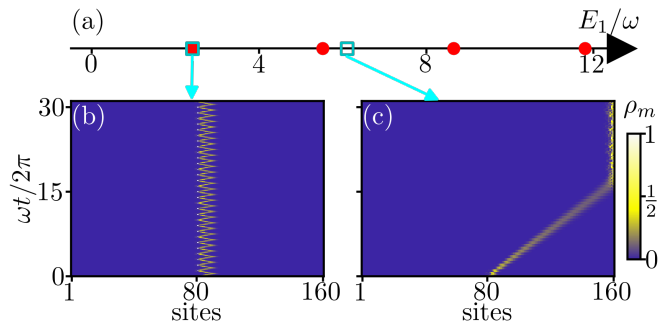


Figure 2: (a) Red round dots are zeros of zeroth order of the Bessel function $\mathcal{J}_0(E_1/\omega)$, which correspond to the condition of the emergence of the dynamic localization under ac field driving. Dynamical evolution of a particle initially localized at the lattice center with (b) $E_1/\omega = 2.405$, which is the first zero point of $\mathcal{J}_0(E_1/\omega)$ and (c) $E_1/\omega = 6.1$. Here we set $J = 1$, $\gamma = 0.73$, and $\omega = 0.46$.

with defective, disordered, quasiperiodic or Stark potentials, or two coupled chains with dissimilar non-reciprocal hoppings [46].

The pure ac electric field case.— We then consider the monochromatic cosine shape ac electric field $E(t) = E_1 \cos(\omega t)$. It is a typical Floquet driving system, with period $T = 2\pi/\omega$. From Eq. (4) and Eq. (6), we have $u(t) = \int_0^t dt' \cos(\frac{E_1}{\omega} \sin \omega t')$ and $v(t) = \int_0^t dt' \sin(\frac{E_1}{\omega} \sin \omega t')$, and then, Eq. (5) gives the probability in the limit $t \gg T$ [51],

$$\rho_m(t \gg T) \approx \mathcal{J}_{m-n_0}^2 \left(2t\sqrt{J_L J_R} \mathcal{J}_0 \left(\frac{E_1}{\omega} \right) \right) \left(\frac{J_R}{J_L} \right)^{m-n_0}. \quad (9)$$

When $\mathcal{J}_0(E_1/\omega) \neq 0$, $2t\sqrt{J_L J_R} \mathcal{J}_0(E_1/\omega)$ increases linearly to infinity and thus $\mathcal{J}_{m-n_0}(2t\sqrt{J_L J_R} \mathcal{J}_0(E_1/\omega))$ tends to zero, which is completely similar to the case without electric field, suggesting that the NHSE is not affected by the ac field. For the special ac field strength E_1 and frequency ω that satisfy $\mathcal{J}_0(E_1/\omega) = 0$, corresponding to the red round dots in Fig. 2(a), due to $\mathcal{J}_{m-n_0}(0) = \delta_{m-n_0,0}$, the particle initially localized in the bulk will move around the initial position, and thus, the NHSE will be suppressed, as shown in Fig. 2(b). This localization phenomenon is called dynamic localization [54–57], which is distinct from Anderson localization induced by random disorder potential. For most cases, $\mathcal{J}_0(E_1/\omega) \neq 0$, the particle will hop to the boundary eventually as demonstrated in Fig. 2(c). To sum up, when only applying the ac electric field to the system, the NHSE is not affected except for these special parameters of E_1 and ω that causes the dynamic localization, suppressing the NHSE.

The dc+ac electric field case.— We finally consider the effect of dc-ac mixed fields, i.e., $E(t) = E_0 + E_1 \cos(\omega t)$, in manipulating NHSE. By using Eq. (4) and Eq. (6), we

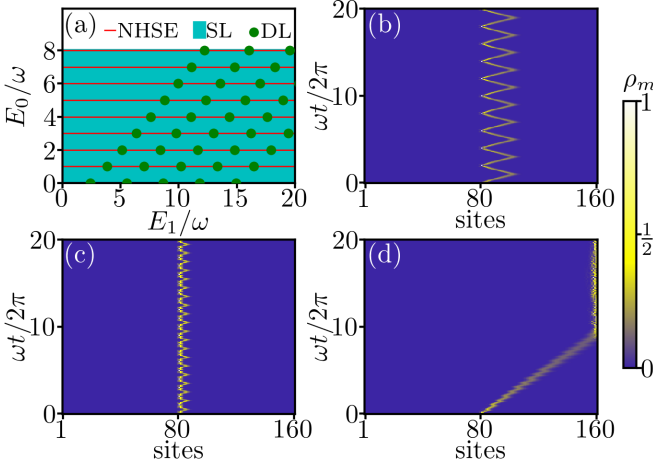


Figure 3: (a) The schematic phase diagram about the existence or non-existence of NHSE under the mixed electric field driving. Red lines represent the integer E_0/ω . Dark green dots on the red lines correspond to E_1/ω being the zeroes of $\mathcal{J}_{E_0/\omega}$, where dynamic localization (DL) induced by the ac field occurs. The light green region correspond to the Stark localization (SL). The dynamical evolutions of the electron initialized on the lattice center under simultaneous driving of dc and ac fields with (b) $E_0/\omega = 0.5$ and $E_1/\omega = 1.3$, (c) $E_0/\omega = 1$ and $E_1/\omega = 3.832$ corresponding to the first zero of \mathcal{J}_1 , and (d) $E_0/\omega = 1$ and $E_1/\omega = 5.7$. Here we fix $J = 1$, $\gamma = 0.73$ and $\omega = 0.46$.

can calculate functions $u(t)$ and $v(t)$, whose expressions look fair complicated [51], and find that when E_0/ω is not an integer, all the terms in the expressions of $u(t)$ and $v(t)$ are bounded oscillatory functions of time, meaning that the particle will oscillate around the initial position. Therefore, the electric fields break NHSE for non-integer E_0/ω . When E_0/ω is an integer, the probability in the limit of long evolution time [51] can be simplified to

$$\rho_m(t \gg T) \approx \mathcal{J}_{m-n_0}^2 \left(2t\sqrt{J_L J_R} \mathcal{J}_{\frac{E_0}{\omega}} \left(\frac{E_1}{\omega} \right) \right) \left(\frac{J_R}{J_L} \right)^{m-n_0} \quad (10)$$

Similar to the discussions for Eq. (S31), the disappearance or existence of NHSE depends on whether E_1/ω is one of the zeroes of the Bessel function $\mathcal{J}_{E_0/\omega}$. The pure dc field can cause the Stark localization, which suppresses NHSE. Then adding the ac field $E_1 \cos(\omega t)$ with E_0/ω being integers, the particle can break through the localization barrier and move through the chain accompanied by the photon absorption or emission. Thus, NHSE can exist only for integer E_0/ω but except the situations that E_1/ω are the zeroes of $\mathcal{J}_{E_0/\omega}$, which will induce the dynamic localization, as discussed above. The effects of the dc-ac mixture fields on NHSE are summarized in the Fig. 3(a). The light green region between the red lines and the dark green dots on the red lines respectively correspond to the non-integer E_0/ω and the zeroes of $\mathcal{J}_{E_0/\omega}$ with E_0/ω being integers, which will induce the

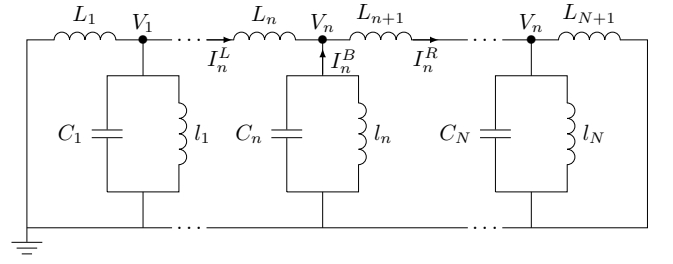


Figure 4: Schematic of the LC electronic circuit.

Stark localization and dynamic localization and lead to the disappearance of NHSE, as shown in Fig. 3(b) and (c). The red lines correspond to the integer E_0/ω , which can break the bulk localization by photon assisted hopping, and the particle initially localized in the bulk will move toward the boundary, as shown in Fig. 3(d).

Electronic circuit's realization.—The non-Hermitian model (1) can be simulated by a classical electric circuit as depicted in Fig. 4, which consists of L LC circuit units. Based on the Kirchoff's current law, we have

$$I_n^R = I_n^L + I_n^B, \quad (11)$$

where I_n^B is the current flows through the n th unit and I_n^L (I_n^R) is the current from the $(n-1)$ th (n th) unit to the n th ($(n+1)$ th) unit, and they satisfy

$$L_n \frac{dI_n^L}{dt} = V_n - V_{n-1}, \quad L_{n+1} \frac{dI_n^R}{dt} = V_{n+1} - V_n, \quad (12)$$

$$l_n \frac{d}{dt} \left[I_n^B - C_n \frac{dV_n}{dt} \right] = V_n, \quad (13)$$

where V_n is the voltage on the node n . From Eqs. (11-13), one can obtain,

$$\frac{d^2 V_n}{dt^2} = \frac{V_{n+1} - V_n}{C_n L_{n+1}} + \frac{V_{n-1} - V_n}{C_n L_n} - \frac{V_n}{C_n l_n} \quad (14)$$

When choosing inductors with inductances $L_n = L_0 g^{-n}$, $l_n = L_n / (\Delta - a n E_0)$, and capacitors with capacitance $C_n = C_0 g^n$, Eq. (14) becomes

$$\left(1 + g + \Delta + \frac{1}{\omega_0^2} \frac{d^2}{dt^2} \right) V_n = V_{n-1} + g V_{n+1} + n a E_0 V_n, \quad (15)$$

where $\omega_0 = 1/\sqrt{C_0 L_0}$. We make a transformation: $V_n \rightarrow V_n e^{\pm i \omega t}$ with $n = 1, 2, \dots, L$ and $\omega = \omega_0 \sqrt{(1 + g + \Delta) - E_R}$, then Eq. (15) becomes $E_R V_n = V_{n-1} + g V_{n+1} + n a E_0 V_n$, which describes the dc case of the model (1) with $J_L = 1$ and $J_R = g$. By directly detecting the eigenvalues and eigenstates through an elementary voltage measurement [21], one can detect the manipulation effect of dc field.

We note that our results can also apply to the manipulation of the NHSE induced by the on-site dissipations. Recent experiment [24] and theoretical proposals [58, 59]

suggest realizing and detecting the NHSE in the dissipative ultracold atom systems, where the gradient fields can be easily realized [60–62]. Therefore, the control effect of the electric fields on the NHSE can be detected in optical lattices. Furthermore, this control effect can also be detected based on the photonic quantum walk [19] and the sideband cooling setups in trapped ion systems [63, 64].

Summary and discussion. — We have investigated the control effect of electric fields on NHSE analytically and numerically. For the pure dc field case, in the thermodynamic limit, a weak Stark localization induced by the dc field is sufficient to win the competition with NHSE, so a non-zero dc field can suppress the NHSE. When the system size is finite, the new interesting phenomenon of the size-dependent NHSE will emerge, because the number of skin modes is size-independent when the size exceed a critical value. For the pure ac field case, only the special field strength E_1 and frequency ω that satisfy $\mathcal{J}_0(E_1/\omega) = 0$ can suppress the NHSE due to the dynamic localization. For the mixed field case, if E_0/ω is not an integer, the NHSE will be suppressed by the Stark localization induced by the dc field. For the integer E_0/ω , NHSE can exist, because the particle can move toward the boundary by the photon absorption or emission except for the special case with E_1/ω being one of the zeroes of $\mathcal{J}_{E_0/\omega}$, which causes the dynamic localization.

The control effects of electric fields on the NHSE are abundant, and moreover, electric fields can be easily applied to a system. Thus, the manipulation methods can be widely used in experiments and the fabrication of new devices. For instance, based on the phenomenon of the size-dependent NHSE and the sensitivity of the NHSE versus the field strength and frequency of ac fields near the special situations that satisfy $\mathcal{J}_0(E_1/\omega) = 0$, by detecting the signals on the boundary of a non-Hermitian system, one can carry out accurate measurements of electric fields, which are important for many critical applications in science and industry. As a second example, the NHSE can be used to design some devices, such as directional amplifiers [65–72] and light funnels [20]. The appearance or disappearance of the directional amplification and the funneling effect can be manipulated by using dc or ac fields, such as by changing the strength or frequency of an added ac field. Thus, one can design the switch of these devices by using electric fields.

We thank L. Li and H. Jiang for valuable discussions. This work was supported by the National Natural Science Foundation of China (Grants No. U1801661, No.12104205, No.12104210), the Key-Area Research and Development Program of Guangdong Province (Grant No. 2018B030326001), Guangdong Provincial Key Laboratory (Grant No.2019B121203002).

* These authors contribute equally to this work.

† Corresponding author: wangyc3@sustech.edu.cn

- [1] Y. Ashida, Z. Gong, and M. Ueda, Non-Hermitian physics, *Advances in Physics* **69**, 249 (2020).
- [2] C. M. Bender and S. Boettcher, Real spectra in non-Hermitian Hamiltonians having PT-symmetry, *Phys. Rev. Lett.* **80**, 5243 (1998); C. M. Bender, D. C. Brody, and H. F. Jones, Complex extension of quantum mechanics, *Phys. Rev. Lett.* **89**, 270401 (2002).
- [3] N. Hatano and D. R. Nelson, Vortex pinning and non-Hermitian quantum mechanics, *Phys. Rev. B* **56**, 8651 (1997); N. Hatano and D. R. Nelson, Non-Hermitian delocalization and eigenfunctions, *Phys. Rev. B* **58**, 8384 (1998).
- [4] T. E. Lee, Anomalous edge state in a non-Hermitian lattice, *Phys. Rev. Lett.* **116**, 133903 (2016).
- [5] H. Shen, B. Zhen, and L. Fu, Topological band theory for non-Hermitian Hamiltonians, *Phys. Rev. Lett.* **120**, 146402 (2018).
- [6] Z. Gong, Y. Ashida, K. Kawabata, K. Takasan, S. Higashikawa, and M. Ueda, Topological phases of non-Hermitian systems, *Phys. Rev. X* **8**, 031079 (2018).
- [7] S. Yao and Z. Wang, Edge states and Topological invariants of non-Hermitian systems, *Phys. Rev. Lett.* **121**, 086803 (2018); S. Yao, F. Song, and Z. Wang, Non-Hermitian Chern bands, *Phys. Rev. Lett.* **121**, 136802 (2018).
- [8] F. K. Kunst, E. Edvardsson, J. C. Budich, and E. J. Bergholtz, Biorthogonal bulk-boundary correspondence in non-Hermitian systems, *Phys. Rev. Lett.* **121**, 026808 (2018).
- [9] Z. Yang, K. Zhang, C. Fang, and J. Hu, Non-Hermitian bulk-boundary correspondence and auxiliary generalized Brillouin zone theory, *Phys. Rev. Lett.* **125**, 226402 (2020).
- [10] C. H. Lee and R. Thomale, Anatomy of skin modes and topology in non-Hermitian systems, *Phys. Rev. B* **99**, 201103 (2019).
- [11] K. Kawabata, K. Shiozaki, M. Ueda, and M. Sato, Symmetry and topology in non-Hermitian physics, *Phys. Rev. X* **9**, 041015 (2019).
- [12] S. Longhi, Topological Phase Transition in non-Hermitian Quasicrystals, *Phys. Rev. Lett.* **122**, 237601 (2019); S. Longhi, Phase transitions in a non-Hermitian Aubry-Andre-Harper model, *Phys. Rev. B* **103**, 054203 (2021).
- [13] H. Jiang, L.-J. Lang, C. Yang, S.-L. Zhu, and S. Chen, Interplay of non-Hermitian skin effects and Anderson localization in non-reciprocal quasiperiodic lattices, *Phys. Rev. B* **100**, 054301 (2019).
- [14] Y. Liu, X. Jiang, J. Cao, and S. Chen, Non-Hermitian mobility edges in one-dimensional quasicrystals with parity-time symmetry, *Phys. Rev. B* **101**, 174205 (2020); Y. Liu, Y. Wang, Z. Zheng, and S. Chen, Exact non-Hermitian mobility edges in one-dimensional quasicrystal lattice with exponentially decaying hopping and its dual lattice, *Phys. Rev. B* **103**, 134208 (2021).
- [15] L. Zhou, Floquet engineering of topological localization transitions and mobility edges in one-dimensional non-Hermitian quasicrystals, *Phys. Rev. Research*, **3**, 033184 (2021).

- [16] E. J. Bergholtz, J. C. Budich, and F. K. Kunst, Exceptional topology of non-Hermitian systems, *Rev. Mod. Phys.* **93**, 015005 (2021).
- [17] H. Schomerus, Topologically protected midgap states in complex photonic lattices, *Opt. Lett.* **38**, 1912 (2013).
- [18] J. Li, A. K. Harter, J. Liu, L. de Melo, Y. N. Joglekar, and L. Luo. Observation of parity-time symmetry breaking transitions in a dissipative Floquet system of ultracold atoms, *Nat. Commun.* **10**, 855 (2019).
- [19] L. Xiao, T. Deng, K. Wang, G. Zhu, Z. Wang, W. Yi, and P. Xue, Non-Hermitian bulk-boundary correspondence in quantum dynamics, *Nat. Phys.* **16**, 761 (2020).
- [20] S. Weidemann, M. Kremer, T. Helbig, T. Hofmann, A. Stegmaier, M. Greiter, R. Thomale, and A. Szameit, Topological funneling of light, *Science* **368**, 311 (2020).
- [21] T. Helbig, T. Hofmann, S. Imhof, M. Abdelghany, T. Kiessling, L. Molenkamp, C. Lee, A. Szameit, M. Greiter, and R. Thomale, Generalized bulk-boundary correspondence in non-Hermitian topoelectrical circuits, *Nat. Phys.* **16**, 747 (2020).
- [22] X.-X. Zhang and M. Franz, Non-Hermitian exceptional Landau quantization in electric circuits, *Phys. Rev. Lett.* **124**, 046401 (2020).
- [23] W. Zhang, X. Ouyang, X. Huang, X. Wang, H. Zhang, Y. Yu, X. Chang, Y. Liu, D.-L. Deng, and L.-M. Duan, Observation of non-Hermitian topology with nonunitary dynamics of solid-state spins, *Phys. Rev. Lett.* **127**, 090501 (2021).
- [24] Q. Liang, D. Xie, Z. Dong, H. Li, H. Li, B. Gadway, W. Yi, and B. Yan, Observation of non-Hermitian skin effect and topology in ultracold atoms, arXiv:2201.09478.
- [25] C. Dembowski, H.-D. Gräf, H. L. Harney, A. Heine, W. D. Heiss, H. Rehfeld, and A. Richter, Experimental observation of the topological structure of exceptional points, *Phys. Rev. Lett.* **86**, 787 (2001); C. Dembowski, B. Dietz, H.-D. Gräf, H. L. Harney, A. Heine, W. D. Heiss, and A. Richter, Encircling an exceptional point, *Phys. Rev. E* **69**, 056216 (2004).
- [26] J. Wiersig, Enhancing the sensitivity of frequency and energy splitting detection by using exceptional points: application to microcavity sensors for single-particle detection, *Phys. Rev. Lett.* **112**, 203901 (2014).
- [27] W. Hu, H. Wang, P. P. Shum, Y. D. Chong. Exceptional points in a non-Hermitian topological pump. *Phys. Rev. B* **95**, 184306 (2017).
- [28] W. Chen, Ş. K. özdemir, G. Zhao, J. Wiersig, and L. Yang, Exceptional points enhance sensing in an optical microcavity, *Nature (London)* **548**, 192 (2017).
- [29] H. Hodaei, A. U. Hassan, S. Wittek, H. Garcia-Gracia, R. El-Ganainy, D. N. Christodoulides, and M. Khajavikhan, Enhanced sensitivity at higher-order exceptional points, *Nature (London)* **548**, 187 (2017).
- [30] M. Zhang, W. Sweeney, C. W. Hsu, L. Yang, A. D. Stone, and L. Jiang, Quantum noise theory of exceptional point amplifying sensors, *Phys. Rev. Lett.* **123**, 180501 (2019).
- [31] M.-A. Miri and A. Alù, Exceptional points in optics and photonics, *Science* **363**, eaar7709 (2019).
- [32] Y. Xu, S.-T. Wang, and L.-M. Duan, Weyl exceptional rings in a three-dimensional dissipative cold atomic Gas, *Phys. Rev. Lett.* **118**, 045701 (2017).
- [33] A. Cerjan, S. Huang, M. Wang, K. P. Chen, Y. Chong, and M. C. Rechtsman, Experimental realization of a Weyl exceptional ring, *Nat. Photonics* **13**, 623 (2019).
- [34] C. H. Lee, L. Li, and J. Gong, Hybrid higher-order skin-topological modes in nonreciprocal systems, *Phys. Rev. Lett.* **123**, 016805 (2019).
- [35] K. Kawabata, S. Higashikawa, Z. Gong, Y. Ashida, and M. Ueda, Topological unification of time-reversal and particle-hole symmetries in non-Hermitian physics, *Nat. Commun.* **10**, 297 (2019).
- [36] U. Magnea, Random matrices beyond the Cartan classification, *Journal of Physics A: Mathematical and Theoretical* **41**, 045203 (2008).
- [37] C. C. Wojcik, X.-Q. Sun, T. Bzdušek, and S. Fan, Homotopy characterization of non-Hermitian Hamiltonians, *Phys. Rev. B* **101**, 205417 (2020).
- [38] Z. Li and R. S. K. Mong, Homotopical classification of non-Hermitian band structures, *Phys. Rev. B* **103**, 155129 (2021).
- [39] H. Hu and E. Zhao, Knots and non-Hermitian bloch bands, *Phys. Rev. Lett.* **126**, 010401 (2021).
- [40] C.-H. Liu and S. Chen, Topological classification of defects in non-Hermitian systems, *Phys. Rev. B* **100**,144106(2019); C.-H. Liu, H. Jiang, and S. Chen, Topological classification of non-Hermitian systems with reflection symmetry, *Phys. Rev. B* **99**, 125103 (2019).
- [41] V. M. M. Alvarez, J. E. B. Vargas, and L. E. F. F. Torres, Non-hermitian robust edge states in one dimension: Anomalous localization and eigenspace condensation at exceptional points, *Phys. Rev. B* **97**, 121401 (2018).
- [42] D. S. Borgnia, A. J. Kruchkov, R.-J. Slager, Non-Hermitian boundary modes and topology, *Phys. Rev. Lett.* **124**, 056802 (2020).
- [43] K. Zhang, Z. Yang, and C. Fang, Correspondence between winding numbers and skin modes in non-Hermitian systems, *Phys. Rev. Lett.* **125**, 126402 (2020); K. Zhang, Z. Yang, and C. Fang, Universal non-Hermitian skin effect in two and higher dimensions, arXiv:2102.05059.
- [44] Y. Yi and Z. Yang, Non-Hermitian skin modes induced by on-site dissipations and chiral tunneling effect, *Phys. Rev. Lett.* **125**, 186802 (2020).
- [45] N. Okuma, K. Kawabata, K. Shiozaki, and M. Sato, Topological origin of non-Hermitian skin effects, *Phys. Rev. Lett.* **124**, 086801 (2020).
- [46] L. Li, C. H. Lee, S. Mu, and J. Gong, Critical non-Hermitian skin effect, *Nat. Commun.* **11**, 5491 (2020); L. Li, C. H. Lee, and J. Gong, Impurity induced scale-free localization, *Commun. Phys.* **4**, 42 (2021).
- [47] M. Lu, X.-X. Zhang, and M. Franz, Magnetic suppression of non-Hermitian skin effects, *Phys. Rev. Lett.* **127**, 256402 (2021).
- [48] K. Shao, H. Geng, W. Chen, and D. Y. Xing, Interplay between non-Hermitian skin effect and magnetic field: skin modes suppression, Onsager quantization and *MT* phase transition, arXiv:2111.04412.
- [49] X.-Q. Sun, P. Zhu, and T. L. Hughes, Geometric response and disclination-induced skin effects in non-Hermitian systems, *Phys. Rev. Lett.* **127**, 066401 (2021).
- [50] R. Hamazaki, K. Kawabata, and M. Ueda, Non-Hermitian many-body localization, *Phys. Rev. Lett.* **123**, 090603 (2019).
- [51] See Supplemental Material for details on (I) deriving the analytical solutions of quantum dynamics; (II) discussing the analytical results; (III) the finite size effect in the pure dc field case; (IV) dynamical behavior in the absence of external fields. The Supplemental Materials includes the references [52, 73, 74].
- [52] G. N. Watson, *A Treatise on the Theory of Bessel Functions*

- tions, Cambridge Mathematical Library (Cambridge University Press, 1995).
- [53] G. H. Wannier, Dynamics of band electrons in electric and magnetic fields, *Rev. Mod. Phys.* **34**, 645 (1962).
- [54] D. H. Dunlap and V. M. Kenkre, Dynamic localization of a charged particle moving under the influence of an electric field, *Phys. Rev. B* **34**, 3625 (1986); D. H. Dunlap and V. M. Kenkre, Dynamic localization of a particle in an electric field viewed in momentum space: Connection with Bloch oscillations, *Phys. Lett. A* **127**, 438 (1988).
- [55] X.-G. Zhao, R. Jahnke, and Q. Niu, Dynamic fractional stark ladders in dc-ac fields, *Physics Letters A* **202**, 297 (1995); X.-G. Zhao, G. A. Georgakis, and Q. Niu, Rabi oscillations between Bloch bands, *Phys. Rev. B* **54**, 5235 (1996).
- [56] S. Longhi, M. Marangoni, M. Lobino, R. Ramponi, P. Laporta, E. Cianci, and V. Foglietti, Observation of dynamic localization in periodically curved waveguide arrays, *Phys. Rev. Lett.* **96**, 243901 (2006).
- [57] A. Eckardt, M. Holthaus, H. Lignier, A. Zenesini, D. Ciampini, O. Morsch, and E. Arimondo, Exploring dynamic localization with a Bose-Einstein condensate, *Phys. Rev. A* **79**, 013611 (2009).
- [58] S. Guo, C. Dong, F. Zhang, J. Hu, and Z. Yang, Theoretical prediction of non-Hermitian skin effect in ultracold atom systems, arXiv:2111.04220.
- [59] L. Zhou, H. Li, W. Yi, and X. Cui, Engineering non-Hermitian skin effect with band topology in ultracold gases, arXiv:2111.04196.
- [60] C. Sias, H. Lignier, Y. P. Singh, A. Zenesini, D. Ciampini, O. Morsch, and E. Arimondo, Observation of photon-assisted tunneling in optical lattices, *Phys. Rev. Lett.* **100**, 040404 (2008).
- [61] H. Miyake, G. A. Siviloglou, C. J. Kennedy, W. C. Burton, and W. Ketterle, Realizing the Harper Hamiltonian with laser-assisted tunneling in optical lattices, *Phys. Rev. Lett.* **111**, 185302 (2013).
- [62] M. Aidelsburger, M. Atala, M. Lohse, J. T. Barreiro, B. Paredes, and I. Bloch, Realization of the Hofstadter Hamiltonian with ultracold atoms in optical lattices, *Phys. Rev. Lett.* **111**, 185301 (2013).
- [63] D. Leibfried, R. Blatt, C. Monroe, and D. Wineland, Quantum dynamics of single trapped ions, *Rev. Mod. Phys.* **75**, 281 (2003).
- [64] Z. Wang, Y. Peng, Y. Lu, Y. Wang, and J. Jie (unpublished).
- [65] A. Metelmann and A. A. Clerk, Nonreciprocal photon transmission and amplification via reservoir engineering, *Phys. Rev. X* **5**, 021025 (2015).
- [66] K. Fang, J. Luo, A. Metelmann, M. H. Matheny, F. Marquardt, A. A. Clerk, and O. Painter, Generalized nonreciprocity in an optomechanical circuit via synthetic magnetism and reservoir engineering, *Nature Phys.* **13**, 465 (2017).
- [67] G. A. Peterson, F. Lecocq, K. Cicak, R. W. Simmonds, J. Aumentado, and J. D. Teufel, Demonstration of efficient nonreciprocity in a microwave optomechanical circuit, *Phys. Rev. X* **7**, 031001 (2017).
- [68] S. Barzanjeh, M. Aquilina, and A. Xuereb, Manipulating the flow of thermal noise in quantum devices, *Phys. Rev. Lett.* **120**, 060601 (2018).
- [69] A. McDonald, T. Pereg-Barnea, and A. A. Clerk, Phase-dependent chiral transport and effective non-hermitian dynamics in a bosonic Kitaev-Majorana chain, *Phys. Rev. X* **8**, 041031 (2018).
- [70] D. Malz, L. D. Tóth, N. R. Bernier, A. K. Feofanov, T. J. Kippenberg, and A. Nunnenkamp, Quantum-limited directional amplifiers with optomechanics, *Phys. Rev. Lett.* **120**, 023601 (2018).
- [71] H. Xu, L. Jiang, A. A. Clerk, and J. G. E. Harris, Nonreciprocal control and cooling of phonon modes in an optomechanical system, *Nature* **568**, 65 (2019).
- [72] W.-T. Xue, M.-R. Li, Y.-M. Hu, F. Song, and Z. Wang, Simple formulas of directional amplification from non-Bloch band theory, *Phys. Rev. B* **103**, L241408 (2021).
- [73] R. B. Paris, An Inequality for the Bessel Function $J_\nu(x)$, *SIAM J. Math. Anal.*, **15**, 203 (1984).
- [74] F. W. J. Olver, D. W. Lozier, and R. F. Boisvert, NIST handbook of mathematical functions, (Cambridge University Press, 2010).

Supplementary Material: Manipulating non-Hermitian skin effect via electric field

In the Supplementary Materials, we first give the details of deriving the analytical solutions of quantum dynamics. Then, we discuss the analytical results and obtain the effects of the pure dc field, pure ac field and the mixed field on the non-Hermitian skin effect. Finally, we discuss the finite size effect in the pure dc field case and the dynamical behavior in the absence of external fields.

I. Analytical solutions of quantum dynamics

We derive the analytical solutions of quantum dynamics for our one-dimensional non-Hermitian model driven by an arbitrary time-dependent electric field $E(t)$. The Hamiltonian are following,

$$\hat{H}(t) = \sum_{m=-\infty}^{+\infty} (J_L|m\rangle\langle m+1| + J_R|m+1\rangle\langle m|) + E(t) \sum_{m=-\infty}^{+\infty} m|m\rangle\langle m|, \quad (\text{S1})$$

where J_R and J_L are the strengths of the leftforward and rightforward hopping, respectively. We expand the time-dependent quantum state as $|\psi(t)\rangle = \sum_{m=-\infty}^{+\infty} C_m(t)|m\rangle$ and substitute it into Schrödinger equation $i\partial_t|\psi(t)\rangle = \hat{H}(t)|\psi(t)\rangle$ (we set $\hbar = 1$ throughout this Supplementary Material) to arrive at the equation of the time-dependent amplitudes $C_m(t) = \langle m|\psi(t)\rangle$,

$$i\partial_t C_m(t) = J_L C_{m+1}(t) + J_R C_{m-1}(t) + E(t) m C_m(t). \quad (\text{S2})$$

In solving Eq. (S2), we transfer to the momentum space firstly by the discrete Fourier transformation,

$$C_k(t) = \sum_{m=-\infty}^{+\infty} e^{-ikm} C_m(t), \quad (\text{S3})$$

and then we can directly rewrite Eq. (S2) as

$$\partial_t C_k(t) - E(t) \partial_k C_k(t) = -i (J_L e^{ik} + J_R e^{-ik}) C_k(t). \quad (\text{S4})$$

This partial differential equation can be transferred to an ordinary differential equation by the variables transformation

$$p = t, q = k + \eta(t), \quad (\text{S5})$$

with $\eta(t) = \int_0^t E(t') dt'$. This gives rise to $C_k(t) = C(p, \tau)$ with $\tau = q - \eta(p)$ and the chain rule of the derivation of $C(p, \tau)$ over p results in the ordinary differential equation,

$$\begin{aligned} \frac{dC(p, \tau)}{dp} &= \frac{\partial C(p, \tau)}{\partial p} \frac{\partial p}{\partial p} + \frac{\partial C(p, \tau)}{\partial \tau} \frac{\partial \tau}{\partial p}, \\ &= \frac{\partial C(p, \tau)}{\partial p} - E(p) \frac{\partial C(p, \tau)}{\partial \tau}, \\ &= -i (J_L e^{i\tau} + J_R e^{-i\tau}) C(p, \tau), \end{aligned} \quad (\text{S6})$$

where we applied Eq. (S4) to the last step. Eq. (S6) can be solved by integrating p over two sides and then

$$\begin{aligned} C(p, \tau) &= C(0, \tau|_{p=0}) e^{-i \int_0^p [J_L e^{i(q-\eta(p'))} + J_R e^{-i(q-\eta(p'))}] dp'}, \\ &= C(0, \tau|_{p=0}) e^{-i \int_0^p [(J_L + J_R) \cos(q-\eta(p')) + i(J_L - J_R) \sin(q-\eta(p'))] dp'}, \\ &= C(0, q) e^{-i \int_0^p [J_+ \cos(q-\eta(p')) + iJ_- \sin(q-\eta(p'))] dp'}, \end{aligned} \quad (\text{S7})$$

where $J_{\pm} = J_L \pm J_R$. Transferring Eq. (S7) back to the form with variables (k, t) yields the solution of Eq. (S4),

$$C_k(t) = C_{k+\eta(t)}(0) e^{-i \int_0^t [J_+ \cos(k+\eta(t)-\eta(t')) + iJ_- \sin(k+\eta(t)-\eta(t'))] dt'}. \quad (\text{S8})$$

To simplify the solutions, we define the following functions

$$\mathcal{U}(t) = \int_0^t \cos[\eta(t) - \eta(t')] dt', \quad (\text{S9})$$

$$\mathcal{V}(t) = \int_0^t \sin[\eta(t) - \eta(t')] dt', \quad (\text{S10})$$

and the Eq. (S8) arrives at

$$\begin{aligned} C_k(t) &= C_{k+\eta(t)}(0) e^{-i[J_+(\mathcal{U} \cos k - \mathcal{V} \sin k) + iJ_-(\mathcal{U} \sin k + \mathcal{V} \cos k)] dt'}, \\ &= C_{k+\eta(t)}(0) e^{i(\bar{\mathcal{V}} \sin k - \bar{\mathcal{U}} \cos k)}. \end{aligned} \quad (\text{S11})$$

where

$$\bar{\mathcal{U}}(t) = J_+ \mathcal{U}(t) + iJ_- \mathcal{V}(t), \quad \bar{\mathcal{V}}(t) = J_+ \mathcal{V}(t) - iJ_- \mathcal{U}(t). \quad (\text{S12})$$

We apply the following expansions, which is expanded by ordinary Bessel functions $\mathcal{J}_m(x)$, to Eq. (S11) [1],

$$e^{-i\bar{\mathcal{U}} \cos k} = \sum_{m=-\infty}^{+\infty} e^{-i\frac{m\pi}{2}} e^{imk} \mathcal{J}_m(\bar{\mathcal{U}}), \quad (\text{S13})$$

$$e^{i\bar{\mathcal{V}} \sin k} = \sum_{m=-\infty}^{+\infty} e^{imk} \mathcal{J}_m(\bar{\mathcal{V}}), \quad (\text{S14})$$

and transfer the solutions in Eq. (S11) back to the spatial space by the discrete Fourier transformation,

$$C_m(t) = \sum_k e^{ikm} C_k(t). \quad (\text{S15})$$

Thus the time-dependent amplitude in spatial space $C_m(t)$ are

$$\begin{aligned} C_m(t) &= \sum_k e^{ikm} C_{k+\eta(t)}(0) e^{i(\bar{\mathcal{V}} \sin k - \bar{\mathcal{U}} \cos k)}, \\ &= \sum_k \sum_{n,r=-\infty}^{+\infty} e^{ik(m+n+r)} C_{k+\eta(t)}(0) e^{-i\frac{n\pi}{2}} J_n(\bar{\mathcal{U}}) J_r(\bar{\mathcal{V}}), \\ &= \sum_k \sum_{n,r=-\infty}^{+\infty} e^{i(k+\eta(t))r} C_{k+\eta(t)}(0) e^{-i\eta(t)r} e^{-i\frac{n\pi}{2}} J_n(\bar{\mathcal{U}}) J_{r-n-m}(\bar{\mathcal{V}}), \\ &= \sum_{n,r=-\infty}^{+\infty} C_r(0) e^{-i\eta(t)r} e^{-i\frac{n\pi}{2}} J_n(\bar{\mathcal{U}}) J_{r-n-m}(\bar{\mathcal{V}}), \\ &= \sum_{n,r=-\infty}^{+\infty} C_r(0) e^{-i\eta(t)r} e^{-i\frac{n\pi}{2}} J_n(\bar{\mathcal{U}}) e^{-i(n+m-r)\pi} J_{n+m-r}(\bar{\mathcal{V}}), \\ &= \sum_{r=-\infty}^{+\infty} (-1)^{m-r} C_r(0) e^{-i\eta(t)r} \left[\sum_{n=-\infty}^{+\infty} J_n(\bar{\mathcal{U}}) J_{n+m-r}(\bar{\mathcal{V}}) e^{i\frac{n\pi}{2}} \right], \\ &= \sum_{r=-\infty}^{+\infty} (-1)^{m-r} C_r(0) e^{-i\eta(t)r} \left(\frac{\bar{\mathcal{V}} + i\bar{\mathcal{U}}}{\bar{\mathcal{V}} - i\bar{\mathcal{U}}} \right)^{\frac{m-r}{2}} J_{m-r} \left(\sqrt{\bar{\mathcal{U}}^2 + \bar{\mathcal{V}}^2} \right). \end{aligned} \quad (\text{S16})$$

In the last step, we applied the Graf's addition theorem of the Bessel functions [1]. Through the relations in Eq. (S12), we can straightforwardly obtain that

$$\frac{\bar{\mathcal{V}} + i\bar{\mathcal{U}}}{\bar{\mathcal{V}} - i\bar{\mathcal{U}}} = \frac{J_R i\mathcal{V} - \mathcal{U}}{J_L i\mathcal{V} + \mathcal{U}}, \quad \bar{\mathcal{U}}^2 + \bar{\mathcal{V}}^2 = 2\sqrt{J_L J_R (\mathcal{U}^2 + \mathcal{V}^2)} = 2\sqrt{J_L J_R (u^2 + v^2)}. \quad (\text{S17})$$

Those expressions simplify the solution of Eq. (S16) to

$$C_m(t) = \sum_{n=-\infty}^{+\infty} (-1)^{m-n} C_n(0) e^{-i\eta(t)n} J_{m-n} \left(2\sqrt{J_L J_R [\mathcal{U}^2(t) + \mathcal{V}^2(t)]} \right) \left[\frac{J_R i\mathcal{V}(t) - \mathcal{U}(t)}{J_L i\mathcal{V}(t) + \mathcal{U}(t)} \right]^{\frac{m-n}{2}}. \quad (\text{S18})$$

This solution is valid for arbitrary initial state and for any time-dependent driven $f(t)$, and also can be specified to the system with finite long chains.

II. Discussions of the analytical results

Base on the exact analytical solution of quantum evolution in Eq. (S18), we can study the properties of the skin-effect and the electric fields induced Wannier Stark localization by choosing an appropriate initial state. Here, we set the system in site $m = 0$ as the specific initial state, i.e., $C_{m=0}(t = 0) = 1$, this is equivalent to set any other sites $m \neq 0$ as the initial state for the infinity long chain. Therefore, we can simplify the solution in Eq. (S18) and explicitly express the probability as,

$$\rho_m(t) = |C_m(t)|^2 = \mathcal{J}_m^2 \left(2\sqrt{J_L J_R [u^2(t) + v^2(t)]} \right) \left(\frac{J_R}{J_L} \right)^m, \quad (\text{S19})$$

where we used the relation $\mathcal{U}^2 + \mathcal{V}^2 = u^2 + v^2$ and here

$$u(t) = \int_0^t dt' \cos \eta(t'), \quad v(t) = \int_0^t dt' \sin \eta(t'). \quad (\text{S20})$$

We note that Eq. (S19) will become Eq.(5) of the main text when we choose the initial state localized at n_0 , i.e., $C_{m=n_0}(t = 0) = 1$ instead of $C_{m=0}(t = 0) = 1$. The exact solutions in Eq. (S19) are valid when $J_L J_R \neq 0$ and project to Hermitian case when $J_L = J_R$. In the Non-Hermitian cases $J_L \neq J_R$, the coefficients $(J_R/J_L)^m$ are responsible to the skin effect. Eq. (S19) is normalized for the Hermitian case, and for non-Hermitian cases, the addition normalization is needed.

Next, we consider the following electric fields

$$E(t) = E_0 + E_1 \cos \omega t, \quad (\text{S21})$$

where E_0 and E_1 are the strengths for the dc and ac parts, respectively. ω is the ac driven frequency. Under this driven, we have

$$\eta(t) = E_0 t + \frac{E_1}{\omega} \sin \omega t, \quad (\text{S22})$$

and then

$$u(t) = \int_0^t dt' \cos \left(E_0 t' + \frac{E_1}{\omega} \sin \omega t' \right), \quad v(t) = \int_0^t dt' \sin \left(E_0 t' + \frac{E_1}{\omega} \sin \omega t' \right). \quad (\text{S23})$$

$u(t)$ and $v(t)$ are not bounded functions only in the absence of electric fields, namely $E(t) = 0$. In this case, we have $u(t) = t$ and $v(t) = 0$, yielding $\rho_m(t) = \mathcal{J}_m^2 (2t\sqrt{J_L J_R}) (J_R/J_L)^m$, which gives purely skin effect due to the argument x in $\mathcal{J}_m(x)$ is linearly increasing to infinity and then $\mathcal{J}_m(x)$ approaches to vanish, such that only the probabilities of the edge sites survive by the coefficients $(J_R/J_L)^m$. This purely skin effect is shown in Fig. S1(b) through the quantum dynamic and as a comparison, the Hermitian case is shown in Fig. S1(a).

DC electric field

For this time-independent driven case $E(t) = E_0$, we have

$$u(t) = \frac{\sin E_0 t}{E_0}, \quad v(t) = \frac{1 - \cos E_0 t}{E_0}, \quad (\text{S24})$$

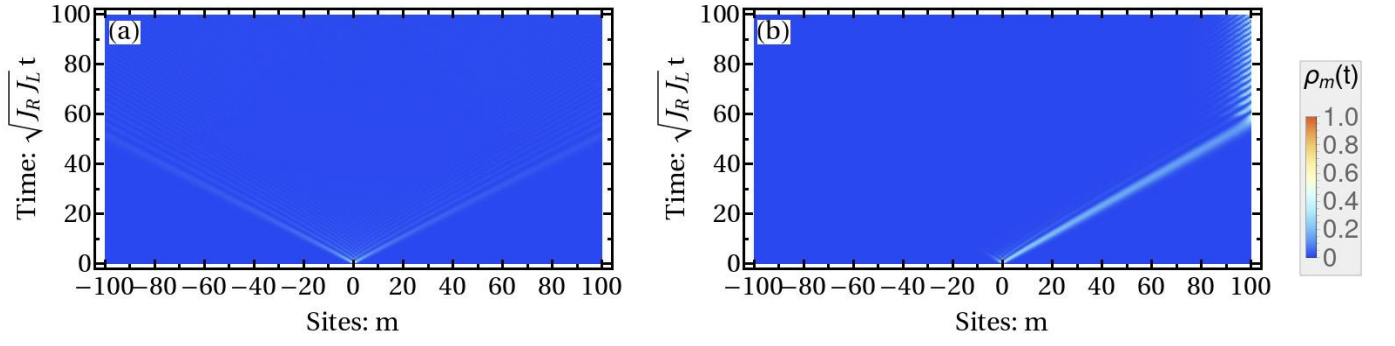


Figure S1: The quantum dynamics in the absence of fields for Hermitian case (a) : $J_L = J_R = 1.0$, and for the Non-Hermitian case (b) : $J_L = 0.8, J_R = 1.0$.

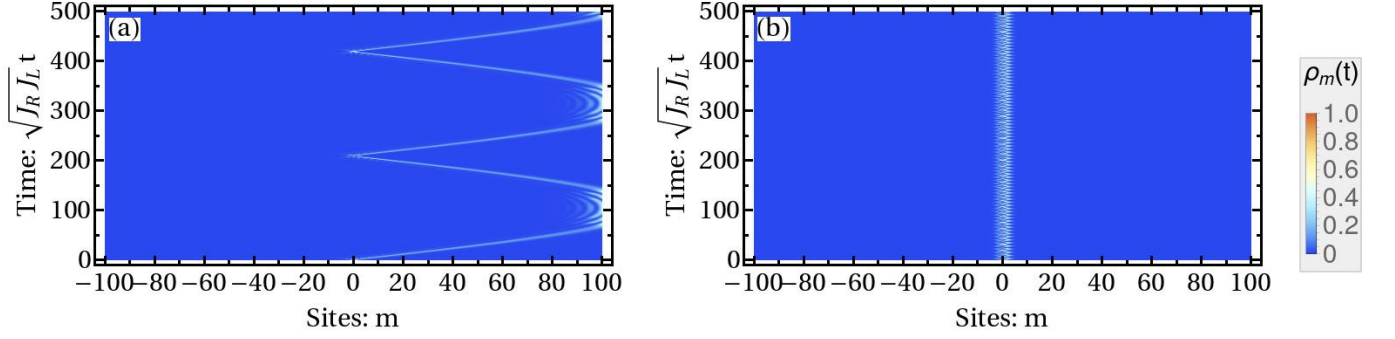


Figure S2: The quantum dynamics for the dc fields with the weakly driven (a) : $E_0 = 0.03$, and the strongly driven (b) : $E_0 = 1.0$. Other parameters are $J_L = 0.8, J_R = 1.0, \omega = 1.0$.

and the probability is

$$\rho_m(t) = \mathcal{J}_m^2 \left(\frac{4\sqrt{J_L J_R}}{E_0} \sin \frac{E_0 t}{2} \right) \left(\frac{J_R}{J_L} \right)^m. \quad (\text{S25})$$

From Eq. (S25), the argument of $\mathcal{J}_m(x)$ is bounded and oscillating along time when $E_0 \neq 0$. It means that the probability amplitude ρ_0 will oscillate back to 1 at the time points $t^* = 2\pi N/E_0$ with $N = 0, 1, 2, \dots$, due to the fact that $\mathcal{J}_m(0) = \delta_{m0}$. This Wannier Stark localization will compete with skin effect under the weakly driven shown in Fig. S2(a), and dominate the dynamics for the strongly driven shown in Fig. S2(b).

AC electric field

For this time-dependent driven case $E(t) = E_1 \cos \omega t$, we have

$$u(t) = \int_0^t dt' \cos \left(\frac{E_1}{\omega} \sin \omega t' \right), \quad v(t) = \int_0^t dt' \sin \left(\frac{E_1}{\omega} \sin \omega t' \right). \quad (\text{S26})$$

At each periodic cycles, i.e., $t^* = 2\pi N/\omega$ with $N = 0, 1, 2, \dots$, we have

$$u(t^*) = \frac{t^*}{\pi} \int_0^\pi d\tau \cos \left(\frac{E_1}{\omega} \sin \tau \right) = t^* \mathcal{J}_0 \left(\frac{E_1}{\omega} \right), \quad v(t) = 0, \quad (\text{S27})$$

and such that the probability at time t^* reads

$$\rho_m(t^*) = \mathcal{J}_m^2 \left(2t^* \sqrt{J_L J_R} \mathcal{J}_0 \left(\frac{E_1}{\omega} \right) \right) \left(\frac{J_R}{J_L} \right)^m, \quad (\text{S28})$$

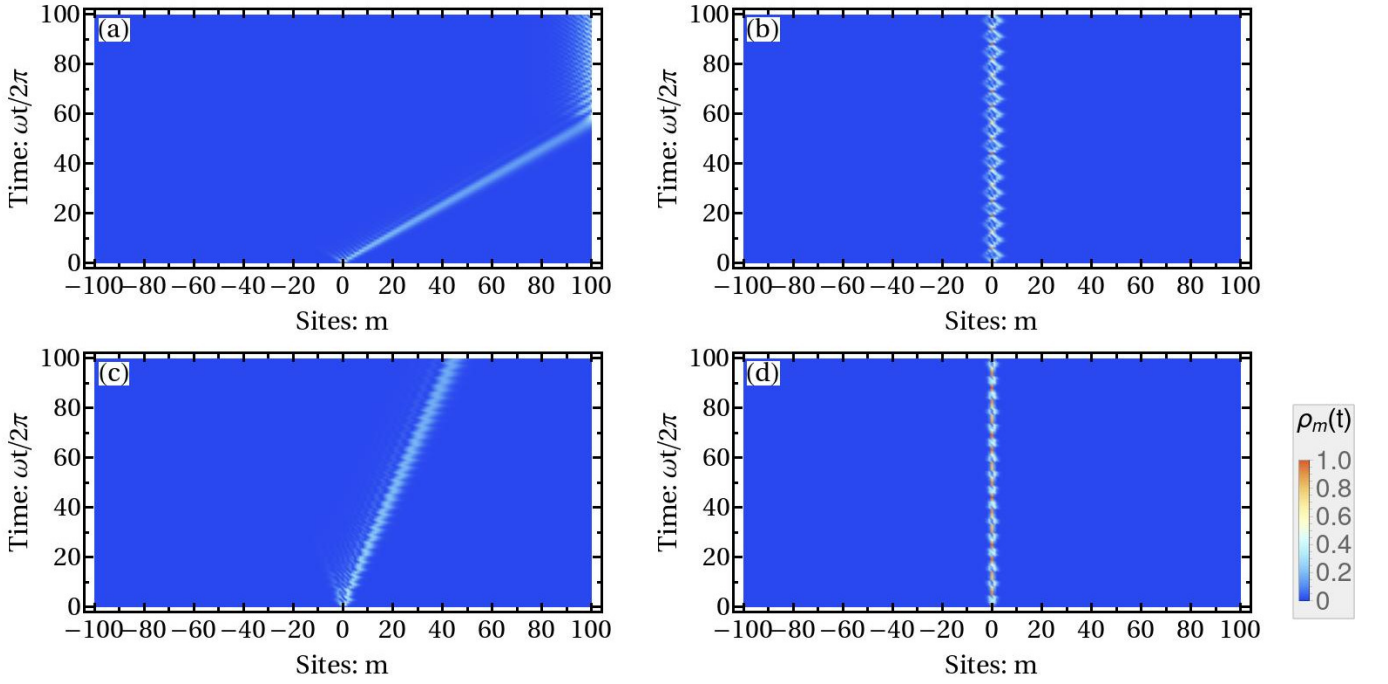


Figure S3: The quantum dynamics for the ac fields with the ratios (a) : $E_1/\omega = 0.1$, (b) : 0.2402 (1st zero of \mathcal{J}_0), (c) : 3.0, (d) : 5.52 (2nd zero of $\mathcal{J}_0(x)$). Other parameters are $J_L = 0.8$, $J_R = 1.0$, $\omega = 1.0$.

where shows that the system is localized only when E_1/ω is the zeros of J_0 , otherwise the skin effect will dominate the dynamics in the long time. To explicitly present this, we define two bounded functions as

$$\bar{u}(t) = u(t) - t\mathcal{J}_0\left(\frac{E_1}{\omega}\right), \quad \bar{v}(t) = v(t) - 0. \quad (\text{S29})$$

Then we rewrite the probability as

$$\rho_m(t) = \mathcal{J}_m^2 \left(2t \sqrt{J_L J_R \left[\mathcal{J}_0^2\left(\frac{E_1}{\omega}\right) + g_1(t)\mathcal{J}_0\left(\frac{E_1}{\omega}\right) + g_2(t) \right]} \right) \left(\frac{J_R}{J_L} \right)^m, \quad (\text{S30})$$

where $g_1(t) = 2\bar{u}(t)/t$ and $g_2(t) = (\bar{u}(t)^2 + \bar{v}(t)^2)/t^2$ are vanished at long time, and then we have

$$\rho_m(t \gg \frac{2\pi}{\omega}) \approx \mathcal{J}_m^2 \left(2t \sqrt{J_L J_R} \mathcal{J}_0\left(\frac{E_1}{\omega}\right) \right) \left(\frac{J_R}{J_L} \right)^m. \quad (\text{S31})$$

In Fig. S3, we take the ratio E_1/ω as two non-zeros of $\mathcal{J}_0(x)$ (a,c) where show the skin effect and as two zeros of $\mathcal{J}_0(x)$ in (b,d) where show the dynamical localization.

DC+AC electric field

The results above show that even weakly dc field will push the system to dynamical localization and while the ac field supports the skin effect except the ratio E_1/ω touches the zeros of Bessel function $\mathcal{J}_0(x)$. The competition between ac and dc fields in regard of localization will significantly modify the behaviors above.

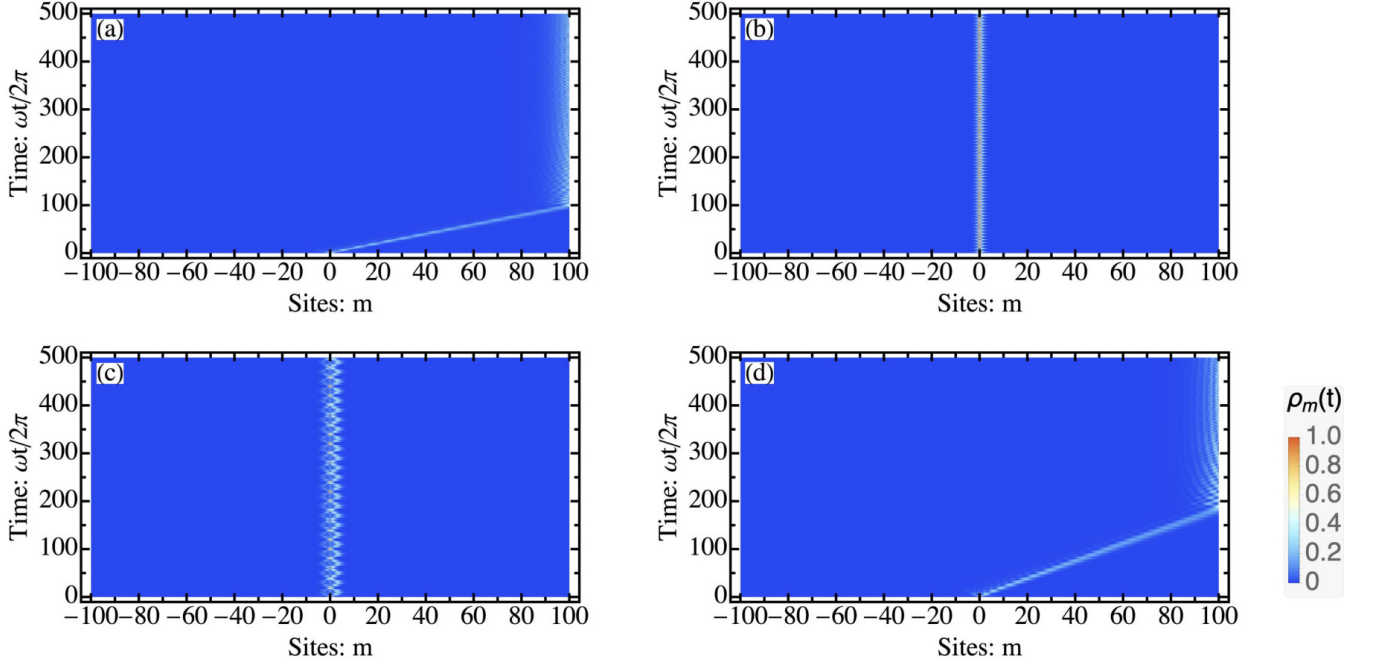


Figure S4: The quantum dynamics for the dc+ac fields with the ratios (a) : $E_0/\omega = 1.0$, $E_1/\omega = 2.0$, (b) : $E_0/\omega = 1.0$, $E_1/\omega = 3.832$ (1st zero of $\mathcal{J}_1(x)$), (c) : $E_0/\omega = 2.324$, $E_1/\omega = 2.0$, (d) : $E_0/\omega = 3.0$, $E_1/\omega = 3.0$. Other parameters are $J_L = 0.8$, $J_R = 1.0$, $\omega = 1.0$.

For this more general case, we firstly rewrite Eq. (S23) as ($\theta = \omega t$)

$$\begin{aligned} u(\theta) &= \frac{1}{\omega} \int_0^{\omega t} d\theta' \cos\left(\frac{E_0}{\omega}\theta' + \frac{E_1}{\omega} \sin\theta'\right), \\ &= \frac{1}{\omega} \int_0^{\omega t} d\theta' \left[\cos\left(\frac{E_0}{\omega}\theta'\right) \cos\left(\frac{E_1}{\omega} \sin\theta'\right) - \sin\left(\frac{E_0}{\omega}\theta'\right) \sin\left(\frac{E_1}{\omega} \sin\theta'\right) \right], \end{aligned} \quad (\text{S32})$$

$$\begin{aligned} v(\theta) &= \frac{1}{\omega} \int_0^{\omega t} d\theta' \sin\left(\frac{E_0}{\omega}\theta' + \frac{E_1}{\omega} \sin\theta'\right), \\ &= \frac{1}{\omega} \int_0^{\omega t} d\theta' \left[\sin\left(\frac{E_0}{\omega}\theta'\right) \cos\left(\frac{E_1}{\omega} \sin\theta'\right) + \cos\left(\frac{E_0}{\omega}\theta'\right) \sin\left(\frac{E_1}{\omega} \sin\theta'\right) \right], \end{aligned} \quad (\text{S33})$$

Applying the following relations [1],

$$\cos(z \sin \theta) = \mathcal{J}_0(z) + 2 \sum_{k=1}^{+\infty} \mathcal{J}_{2k}(z) \cos(2k\theta), \quad \sin(z \sin \theta) = 2 \sum_{k=0}^{+\infty} \mathcal{J}_{2k+1}(z) \sin[(2k+1)\theta], \quad (\text{S34})$$

and doing the integrating, we arrive at

$$u(t) = \frac{\sin(E_0 t)}{E_0} \mathcal{J}_0\left(\frac{E_1}{\omega}\right) + \sum_{k=1}^{+\infty} (-1)^k \mathcal{J}_k\left(\frac{E_1}{\omega}\right) \left[\frac{\sin(E_0 - k\omega)t}{E_0 - k\omega} + \frac{\sin(E_0 + k\omega)t}{E_0 + k\omega} \right], \quad (\text{S35})$$

$$\begin{aligned} v(t) &= \frac{1 - \cos(E_0 t)}{E_0} \mathcal{J}_0\left(\frac{E_1}{\omega}\right) + \frac{2}{\omega} \sum_{k=1}^{+\infty} \mathcal{J}_{2k}\left(\frac{E_1}{\omega}\right) \frac{\frac{E_0}{\omega} - \frac{E_0}{\omega} \cos(E_0 t) \cos(2k\omega t) - 2k \sin(E_0 t) \sin(2k\omega t)}{(\frac{E_0}{\omega})^2 - 4k^2} \\ &\quad + \frac{2}{\omega} \sum_{k=0}^{+\infty} \mathcal{J}_{2k+1}\left(\frac{E_1}{\omega}\right) \frac{-(2k+1) + (2k+1) \cos(E_0 t) \cos[(2k+1)\omega t] + \frac{E_0}{\omega} \sin(E_0 t) \sin((2k+1)\omega t)}{(\frac{E_0}{\omega})^2 - (2k+1)^2}. \end{aligned} \quad (\text{S36})$$

These expressions look very complicated and are difficult in doing the calculations continuously. Even so, we still can do some analysis depends on whether the ratio E_0/ω is an integer or not. If E_0/ω is not an integer, all the terms in

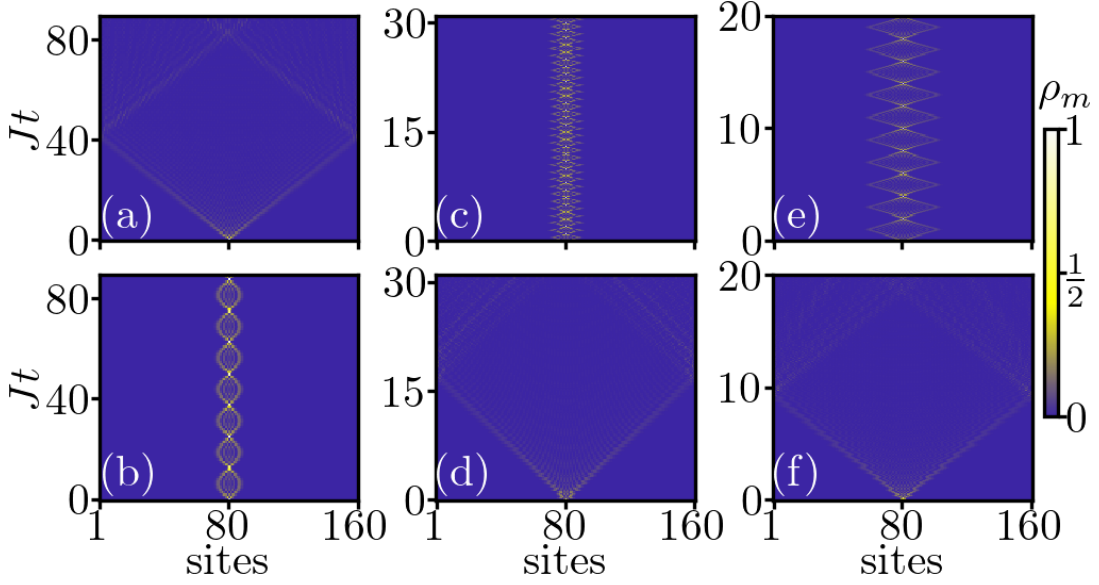


Figure S5: Dynamical evolution of a electron started from the lattice center for the system described by Eq. (S1) with (a) $E_0 = 0.005$, $E_1 = 0$, (b) $E_0 = 0.5$, $E_1 = 0$, (c) $E_0 = 0$, $E_1/\omega = 2.405$, which is the first zero point of $\mathcal{J}_0(E_1/\omega)$, (d) $E_0 = 0$, $E_1/\omega = 6.1$, (e) $E_0/\omega = 0.5$, $E_1/\omega = 1.3$, (f) $E_0/\omega = 1$, $E_1/\omega = 5.7$. Except J_R and J_L , (a),(b) and Fig.1 (e),(f) of the main text have same parameters, (c),(d) and Fig.2 (c),(d) of the main text have same parameters, (e),(f) and Fig.3 (b),(d) of the main text have same parameters. Here $J_R = J_L = 1$.

Eqs. (S35-S36) are bounded oscillatory functions of time such that the system will localize around the initial states. It means that the dc part of electric field dominate over the ac part and then indicate breaking of the skin effect. In the case of provided E_0/ω is an integer, function $v(t)$ in Eq. (S36) will not deduce any non-bounded functions and will have similar contributions as in the integer case. However, the functions $u(t)$ in Eq. (S35) takes (set $E_0 = \nu\omega$, $\nu \in \mathbb{Z}$)

$$u(t) = (-1)^\nu \mathcal{J}_\nu \left(\frac{E_1}{\omega} \right) t + \frac{\sin(E_0 t)}{E_0} \mathcal{J}_0 \left(\frac{E_1}{\omega} \right) + \sum_{k=1, k \neq \nu}^{+\infty} (-1)^k \mathcal{J}_k \left(\frac{E_1}{\omega} \right) \left[\frac{\sin(E_0 - k\omega)t}{E_0 - k\omega} + \frac{\sin(E_0 + k\omega)t}{E_0 + k\omega} \right] \quad (\text{S37})$$

and then the first term is a non-bounded and linearly increasing function of time, such that at long time, we have

$$u(t \gg \frac{2\pi}{\omega}) \approx (-1)^\nu \mathcal{J}_\nu \left(\frac{E_1}{\omega} \right) t, \quad (\text{S38})$$

and the probability

$$\rho_m(t \gg \frac{2\pi}{\omega}) \approx \mathcal{J}_m^2 \left(2t \sqrt{J_L J_R} \mathcal{J}_{\frac{E_0}{\omega}} \left(\frac{E_1}{\omega} \right) \right) \left(\frac{J_R}{J_L} \right)^m, \quad (\text{S39})$$

which is merely replacing the order "0" in Eq. (S31) by E_0/ω .

As a conclusion, in this "dc+ac" case, the system will be featured in dynamical localization for all non-integer ratio E_0/ω (Fig. S4 (c)) and will be dominated by skin effect for all E_1/ω except zeros of $\mathcal{J}_{E_0/\omega}(x)$ when the ratio E_0/ω takes integer (Fig. S4 (a, b, d)). We show the parameters zone for the skin effect by the solid lines in Fig.3(a) in main text and all the rest zone are for dynamical localization.

Hermitian case

To understand the physical picture mentioned in the main text more intuitively, we here provide the time evolution of the corresponding Hermitian case, i.e., $J_R = J_L$, as shown in Fig. S5. Figs. S5 (a),(b) show the dc case, whose parameters are same with Figs.1 (e),(f) of the main text. The previous discussions about the dc case can be directly applied to the $J_R = J_L$ case, as shown in Fig. S5 (b). Although both Fig. S5(b) and Fig.1(f) of the main text show the Stark localization, there also exist the differences. From Fig. S5 (b), the particle oscillate around the initial

position, but when $J_R > J_L$, the oscillation of the particle is at the right-hand side of the initial position [Fig.1(f)]. Comparing Fig. S5(c), Fig.S5(e) and Fig.2(c), Fig.3 (b) of the main text, we can also clearly see the phenomenon that the oscillation center move to the right of the initial position when changing $J_L = J_R$ to $J_L < J_R$.

When E_0 is decreased, as discussed below, the oscillation amplitude will increase. For a finite system, when the oscillation amplitude is larger than the system size, the particle can arrive at the boundary, as shown in Fig. S5 (b). When $J_R > J_L$, the particle will arrive at the boundary and then stay there ever since [Fig.1(e)], which corresponds to the existence of the NHSE. The competition between the oscillation amplitude and the system size induce the phenomenon of the size-dependent NHSE. Comparing Fig. S5(d), Fig.S5(f) and Fig.2(d), Fig.3 (d) of the main text, it can be seen that the extended states become the skin modes when changing $J_L = J_R$ to $J_L < J_R$.

III. Finite size effect for the pure dc case

In this section, we investigate the finite size effect in the pure dc field case. According to the inequality proven by Paris [2] for Bessel function, the probability $\rho_m(t)$ is bounded from above for big enough m ,

$$\rho_m(t) \leq \mathcal{J}_{m-n_0}^2(m-n_0) f_\chi^{2(m-n_0)}(x_t). \quad (\text{S40})$$

Here $f_\chi(x_t) = x_t e^{1-\chi x_t}$, $\chi = \sqrt{J_L/J_R} < 1$, and $x_t = \frac{4J_R}{(m-n_0)|E_0|} \left| \sin \frac{E_0 t}{2} \right|$. The inequality holds if $4\sqrt{J_L J_R} \leq (m-n_0)|E_0|$. $f_\chi(x_t)$ is monotonically increasing and bounded $0 \leq f_\chi(x_t) \leq 1/\chi$, for $0 \leq x_t \leq 1/\chi$. One can calculate the derivation of f_χ to verify it.

$$f'_\chi(x_t) = e^{1-\chi x_t} - \chi x_t e^{1-\chi x_t} = e^{1-\chi x_t} (1 - \chi x_t). \quad (\text{S41})$$

And $f_\chi(x_t = 1) = e^{1-\chi} > 1$ since $\chi < 1$. There exists $0 \leq x_\star < 1$ such that $f_\chi(x_\star) = 1$ and $0 \leq f_\chi(x_t) < 1$ if $0 \leq x_t < x_\star$. Note that x_\star depends only on J_L and J_R , and satisfies $x_\star e^{1-\sqrt{J_L/J_R} x_\star} = 1$. We also know $|\mathcal{J}_n(\bullet)| \leq 1$ [3]. Thus

$$\begin{aligned} \rho_m(t) &\leq \mathcal{J}_{m-n_0}^2(m-n_0) f_\chi^{2(m-n_0)} \left(\frac{4J_R}{(m-n_0)|E_0|} \left| \sin \frac{E_0 t}{2} \right| \right) \\ &\leq \mathcal{J}_{m-n_0}^2(m-n_0) \left[\underbrace{f_\chi \left(\frac{4J_R}{(m-n_0)|E_0|} \right)}_{<1} \right]^{2(m-n_0)} \\ &\leq \left[\underbrace{f_\chi \left(\frac{4J_R}{(m-n_0)|E_0|} \right)}_{<1} \right]^{2(m-n_0)}. \end{aligned} \quad (\text{S42})$$

As m increases, $f_\chi(4J_R/(m-n_0)|E_0|)$ would decrease further. Thus the decay rate of ρ_m is faster than any exponential decay rate as m increases. Hence $\rho_m(t)$ would be insignificant if $4J_R < (m-n_0)|E_0|x_\star$. It is well known that $\mathcal{J}_{-n}(\bullet) = (-1)^n \mathcal{J}_n(\bullet)$. For two sites $2n_0 - m$ (left side $< n_0$) and m (right side $> n_0$) with equal distance to n_0

$$\frac{\rho_{2n_0-m}(t)}{\rho_m(t)} \approx \frac{\mathcal{J}_{n_0-m}^2(2t\sqrt{J_L J_R} \mathcal{J}_0(\frac{E_1}{\omega})) \left(\frac{J_R}{J_L} \right)^{n_0-m}}{\mathcal{J}_{m-n_0}^2(2t\sqrt{J_L J_R} \mathcal{J}_0(\frac{E_1}{\omega})) \left(\frac{J_R}{J_L} \right)^{m-n_0}} = \left(\frac{J_R}{J_L} \right)^{-2(m-n_0)}. \quad (\text{S43})$$

Adding the fact that $J_R > J_L$, $\rho_{2n_0-m}(t)$ would be even less significant, if $m > n_0$ and $4J_R < (m-n_0)|E_0|x_\star$. Therefore, in an infinite lattice, an electron would oscillate around its initial position n_0 within a range of $4J_R/|E_0|x_\star$.

IV. Dynamical behavior of a particle on non-reciprocal tight-binding model with non-Hermitian skin effect

In this section, we take the case without external field as an example to discuss the dynamical behavior of a particle. When there is no electric field, Eq. (S40) and Eq. (S43) would still be valid except $x_t = 2tJ_R/(m-n_0)$. Eq. (S43)

tells us that the electron would always favor the right-hand side of n_0 . Further, from Eq. (S41) we know that $f_\chi(x_t)$ increases from 0 to $f_\chi^{\max} = \sqrt{J_R/J_L}$ as x_t increases from 0 to $1/\chi$. Hence $f_\chi(x_t) < 1$ and thus the upper bound of ρ_m (see Eq. (S40)) would be very small, when $x_t < x_\star$. Here $f_\chi(x_\star) = 1$ and $x_\star < 1$ as mentioned in the previous section. Hence ρ_m would be significant only if $x_t \geq x_\star$, namely

$$t \geq \frac{(m - n_0)x_\star}{2J_R}. \quad (\text{S44})$$

Therefore, the electron reaches site m around $t_a = \frac{(m - n_0)x_\star}{2J_R}$ and continues hopping rightward. Now we consider the stable probability in a long time after the particle passing. As discussed above, in the absence of external fields, $\rho_m(t) = \mathcal{J}_{m-n_0}^2(2t\sqrt{J_L J_R}) (J_R/J_L)^{m-n_0}$, where $2t\sqrt{J_L J_R}$ is linearly increasing to infinity with increasing time, and thus $\mathcal{J}_{m-n_0}^2(2t\sqrt{J_L J_R})$ tends to 0. We consider ρ_m/ρ_{m-1} when $t \rightarrow \infty$. For convenience, we consider the long time averaged behavior after the particle has passed the position m for a long time. We notice that $\frac{\int_{t \gg t_a}^{\infty} dt \mathcal{J}_{m-n_0}^2(2t\sqrt{J_L J_R})}{\int_{t \gg t_a}^{\infty} dt \mathcal{J}_{m-1-n_0}^2(2t\sqrt{J_L J_R})} = 1$ and so $\rho_m/\rho_{m-1} = J_R/J_L$. Thus, for a system with non-Hermitian skin effect, the probability distributions of the region that the particle has passed through are not ergodic, which is obviously different from the system without skin effect.

* These authors contribute equally to this work.

† Corresponding author: wangyc3@sustech.edu.cn

- [1] G. N. Watson, A Treatise on the Theory of Bessel Functions, Cambridge Mathematical Library (Cambridge University Press, 1995).
- [2] R. B. Paris, An Inequality for the Bessel Function $J_\nu(\nu x)$, SIAM J. Math. Anal., **15**, 203 (1984).
- [3] F. W. J. Olver, D. W. Lozier, and R. F. Boisvert, NIST handbook of mathematical functions, (Cambridge University Press, 2010).